Published online 27 April 2020

Nucleic Acids Research, 2020, Vol. 48, No. 11 ***e65***
doi: 10.1093/nar/gkaa303

Encoding multiple digital DNA signals in a single analog channel

Yan Helen Yan [1,2], David Yu Zhang [1,2,*] and Lucia R. Wu [2,*]

[1]Systems, Synthetic, and Physical Biology, Rice University, Houston, 77030 TX, USA and [2]Department of Bioengineering, Rice University, Houston, 77030 TX, USA

Received November 20, 2019; Revised March 06, 2020; Editorial Decision April 16, 2020; Accepted April 17, 2020

ABSTRACT

For many analytic and biomedical applications, the presence of an analyte above or below a critical concentration is more informative for decision making than the actual concentration value. Straightforward analog-to-digital signal conversion does not take full advantage of the precision and dynamic range of modern sensors. Here, we present and experimentally demonstrate an analog-to-multiple-digital signal conversion, reporting digital signals that indicate whether the concentrations of specific DNA sequences exceed respective threshold values. These threshold values can be individually programmed for each target sequence. Experimentally, we showed representation of four DNA targets' information in a single fluorescence channel.

INTRODUCTION

Results of many analytic and biomedical applications are binary; the presence of an analyte above or below a critical concentration is more important for decision making than the actual value. For example, the result of an infectious pathogen test (1,2) is reported qualitatively as positive or negative, and the result of a product quality test is reported as pass or fail. By contrast, most sensors used to measure physical, chemical or biological properties generate analog signals (Figure 1A), e.g. pH meter (3,4), electrochemical sensor (5–7), enzyme-linked immunosorbent assay (8,9) and optical ring resonator (10,11).

Currently two strategies are used to measure multiple properties simultaneously in a test. The first strategy is to split the sample, and then assay each aliquot with a different tool or method. The second strategy is to simultaneously or serially apply multiple sensors to the same sample, e.g. using different optical excitation wavelengths and emission photodetectors, such as multiplex fluorescence-based quantitative polymerase chain reaction (qPCR). Both strategies have significant limitations. The first strategy requires larger sample input volumes and can adversely affect clinical sensitivity when applied to medical diagnostics; the second strategy does not work for many detection modalities, and significantly increases instrument and consumable costs when it is available.

The high-information density of a precise analog signal allows it to be encoded with multiple digital signals. For example, the time of a day can be represented as Hours:Minutes:Seconds, which comprises three separate digital signals. In electronics, analog-to-digital converter (12) has long been used to convert an analog signal such as a sound picked up by a microphone to a digital signal through the process of sampling and quantization, but we are not aware of any implementation of analog-to-multiple-digital signal conversion in chemistry. Here we present a method to map a single analog signal (fluorescence) to multiple digital signals (whether a DNA/RNA marker concentration exceeds a threshold), allowing more efficient use of limited signal channel parameter space to communicate a higher density of information.

Analog to digital signal theory

A system with D independent dimensions has a total of 2^D possible states. If we can divide an analog signal space into 2^D distinct signal levels, then each level can be used to represent a different system state. Therefore, based on the observed analog signal, the system state of all D parameters can be inferred (Figure 1B and C).

In a sensor with linear analog response, the maximum number of levels (N_{Level}) in a signal space is determined by the dynamic range, background, and noise level; it is calculated as $N_{\text{Level}} = (I_{\text{Max}} - I_{\text{BG}})/I_{\text{Noise}}$, where I_{Max} is the maximum signal intensity, I_{BG} is the background signal intensity and I_{Noise} is the intensity of the inherent noise of the sensor, which refers to the minimal signal difference that can be reliably detected by the sensor. Take fluorometer as an example: $I_{\text{Max}} \approx 10^6$ relative fluorescence units (RFU), $I_{\text{BG}} \approx 500$ RFU and I_{Noise} is within 100 RFU, so that $N_{\text{Level}} \approx (10^6 - 500)/100 = 10^4$ states. The maximum dimension number of digital signal (D_{Max}) that can fit into this signal

*To whom correspondence should be addressed. Tel: +1 713 348 5869; Fax: +1 713 348 5877; Email: rw23@rice.edu
Correspondence may also be addressed to David Yu Zhang. Tel: +1 713 348 2832; Fax: +1 713 348 5877; Email: dyz1@rice.edu

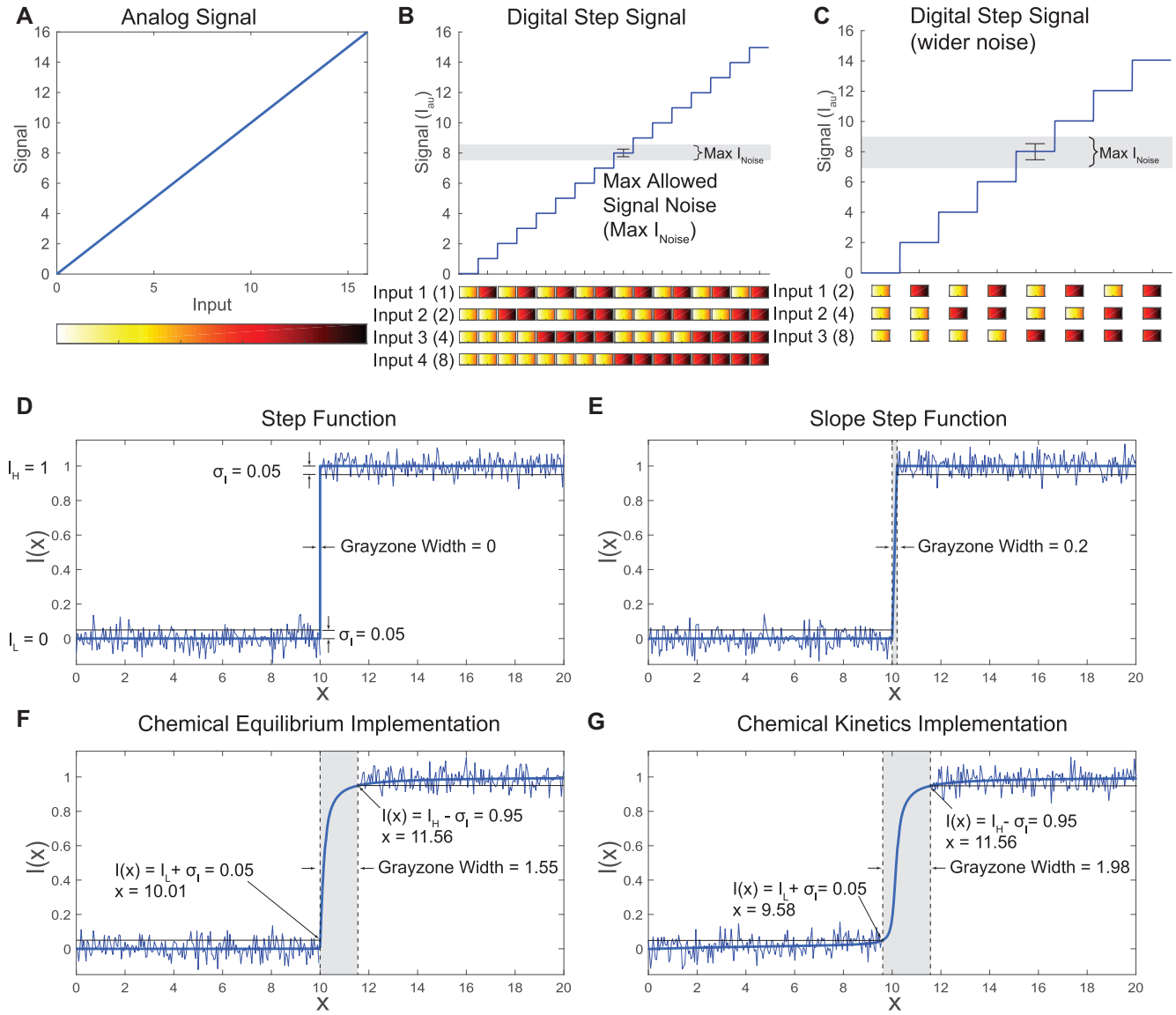

Figure 1. Compressing multiple digital signals into an analog signal channel. (**A**) A typical sensor generates an analog signal response, which is a continuous signal that reflects the amplitude of a single input. (**B**) When the signal response is a step function, the analog signal space can be used as a digital signal space of N different levels; the allowed Maximum Noise (MaxI_{Noise}) of each level is ± step size/2. Binary information (i.e. high/above threshold or low/below threshold) of multiple different inputs can be compressed into this digital signal space. Here is an example of a digital signal space with $N = 16$ levels, which can represent the binary information of a maximum of four different inputs; each of the $2^4 = 16$ possible combinations has a corresponding digital signal level. (**C**) When the MaxI_{Noise} value of the signal increases, distinguishable levels that can fit into the same dynamic range will decrease. The maximum number of distinguishable levels can be calculated as Dynamic Range/MaxI_{Noise}. (**D**) To implement this idea, each input should have a signal response similar to a step function. A step function is a discontinuous function with a baseline value I_{L} for low (<threshold) input and a maximal value I_{H} for high (>threshold) input; a perfect step function has no grayzone (i.e. the range of input generating ambiguous response). Noise with a standard deviation (sd) of 0.05 is shown here. (**E**) Practically, the signal generated by a sensor is more similar to a slope step function than to a step function. The slope step function is a continuous function with a transition region in which the signal linearly increases from the baseline to the maximal value; this transition region is a grayzone. Here the width of the grayzone is 0.2. (**F**) Consider a sensor measuring the concentration of an input analyte based on a chemical reaction, the response is a slope step function only when the reaction free energy $\Delta G^{\circ} = -\infty$. In practice, we expect a smooth function response and a wider grayzone than the slope step function because the ΔG° is not negative enough. The grayzone here is re-defined as: from the input where the signal is above baseline signal + sd to the input where is signal is maximal signal − sd. (**G**) If the signal is measured at a time point where the chemical equilibrium has not been reached, the grayzone will be wider than the equilibrium grayzone.

space is calculated as $D_{\mathrm{Max}} = \mathrm{floor}(\log_2 N_{\mathrm{Level}}) = 13$, indicating that theoretically 13 different dimensions can be expressed in a single fluorescence channel. Sensors with better technical specifications, such as larger I_{Max}, smaller I_{BG} or smaller I_{Noise} allow more distinct analog states, and enable denser encoding of digital signals.

As an initial demonstration of the analog-to-multiple-digital conversion, we consider the representation of whether the concentrations of multiple distinct analytes x_i are above their respective thresholds $\mathrm{Threshold}_i$. In a perfect Heaviside thresholding function (Figure 1D), the input-output response between the concentration [x] and the output signal I_x follows a perfect step function and we will not observe an intermediate value of I_x that lies between the high value I_H and the low value I_L. However, in practice, due to sensor precision limitations, we expect the existence of noise, the intensity of which is depicted as I_{Noise}, but this value should be much smaller than the difference I_H - I_L. If the signal generated by different inputs do not interfere with each other, the observed signal level will be the sum of responses from all inputs.

To implement analog-to-multiple-digital conversion and allow unambiguous communication of each of the 2^D different system states, each step function's $I_{\mathrm{H}} - I_{\mathrm{L}}$ values should be different. Here we recommend using $I_{\mathrm{H}} - I_{\mathrm{L}} = 2^{(k-1)} I_{\mathrm{au}}$ for the step function of the kth dimension, so that the signal levels are evenly spaced (see Supplementary Materials S1 and Figure S1–3 for details); I_{au} is an arbitrary unit of signal that is greater than I_{Noise}. For example, in a $D = 4$ system, the $I_{\mathrm{H}} - I_{\mathrm{L}}$ values are I_{au}, $2I_{\mathrm{au}}$, $4I_{\mathrm{au}}$ and $8I_{\mathrm{au}}$ for each step function; the possible observed signal levels (background subtracted) have $2^D = 16$ unique values that are evenly spaced between $0I_{\mathrm{au}}$ and $15I_{\mathrm{au}}$ (Figure 1B).

In reality, it is difficult to convert an analog response to a digital response with a step function. In slope step function, there is a "grayzone" of analyte concentrations [x] in which the output signal is between I_{L} and I_{H} (Figure 1E). Analyte concentrations in this grayzone range must be avoided, because it will result in incorrect interpretation of the system state from the summed signal. When the grayzone concentration range is small compared to the overall range of possible analyte concentrations, this limitation has limited impact on the overall system. However, we do wish to limit the width of the grayzone through rational design of the chemical reaction, as discussed later.

When using a chemical reaction-based sensor to mimic the slope step function, the signal is generated when the reaction reaches equilibrium; because the chemical reaction yield does not reach 100% when the target concentration reaches above threshold, the transition region from I_{L} to I_{H} becomes wider than on the slope step function (Figure 1F).

$$x + \mathrm{Thresholder} \rightarrow \emptyset \quad (1)$$

$$x + \mathrm{Sensor} \rightarrow I \quad (2)$$

The standard free energy of reaction (1) must be more negative (favorable) than that of reaction (2), in order for the Thresholder chemical to preferentially react with the analyte. The sensor will saturate at a given analyte concentration, resulting in the right side of the step function. The more negative the free energy of reaction (2), the sharper the response curve becomes; at $\Delta G^{\circ} = -\infty$, the response curve completely represents the slope step function. If we further consider a chemical sensor that has not reached equilibrium (which is the case for most sensors), the transition region is wider than that of the equilibrium state (Figure 1G). In these cases, faster kinetics or allowing the reaction to proceed for a longer time will generate sharper response curves.

In this article, we define the range of input (x) that generates signals between $I(x) = I_{\mathrm{L}} + \sigma_I$ and $I(x) = I_{\mathrm{H}} - \sigma_I$ as the grayzone; here σ_I is the standard deviation of noise. The response signal produced by an input value in the grayzone cannot be clearly classified into any of the output states, thus it is essential to minimize the grayzone of every signal dimension.

Theory implementation

In this article, we chose fluorescent probe-based DNA detection assay as a model system. We demonstrated compressed encoding of DNA targets' binary concentration information (i.e. above or below threshold) in a single fluorescence channel; the step-function-like signal response in each dimension was generated using a toehold probe-based (13,14) thresholding mechanism. There are two types of toehold probes in the system: the Reporter (R) and the Trap (Tr); the Trap acts as the Thresholder and the Reporter acts as the Sensor to detect the DNA target (the analyte x). Both probes consist of a Complement (C) strand and a Protector (P) strand. The C strand is complementary to the target, and the P strand is partially complementary to C. The Reporter has a nonhomologous region that does not hybridize to the target, so that the reaction of target hybridizing to Reporter is reversible both thermodynamically and kinetically. The RC strand is modified with a fluorophore and the RP strand is modified with a quencher, so that fluorescence signal is generated when the target displaces the Protector. The Trap does not have a nonhomologous region, so its reaction with the target is minimally reversible; it does not generate fluorescence signal when hybridized to the target (Figure 2A).

Because the target hybridizes to the Trap with a more negative ΔG° than to the Reporter, the target reacts with the Trap more preferably than with the Reporter, and the fluorescence signal is observed only when most of the Trap is consumed. Therefore, the Trap concentration determines the threshold of detection, and the Reporter concentration determines the I_{H} signal of the response function; the I_{L} signal is dependent on the fluorescence quenching ratio of the Reporter. The signal response of this system is similar to a slope step function with a narrow grayzone (Figure 3A). The simulation details are shown in Supplementary Materials S1. When detecting multiple DNA targets simultaneously in one fluorescence channel, every different target has a corresponding pair of Reporter and Trap that both specifically hybridize to the target sequence; all Reporters in the system bear the same fluorophore. Because the toehold probes are highly specific, Reporters and Traps binding to different targets should not have any interactions (13,14), making it easy to deconvolute the compressed signal.

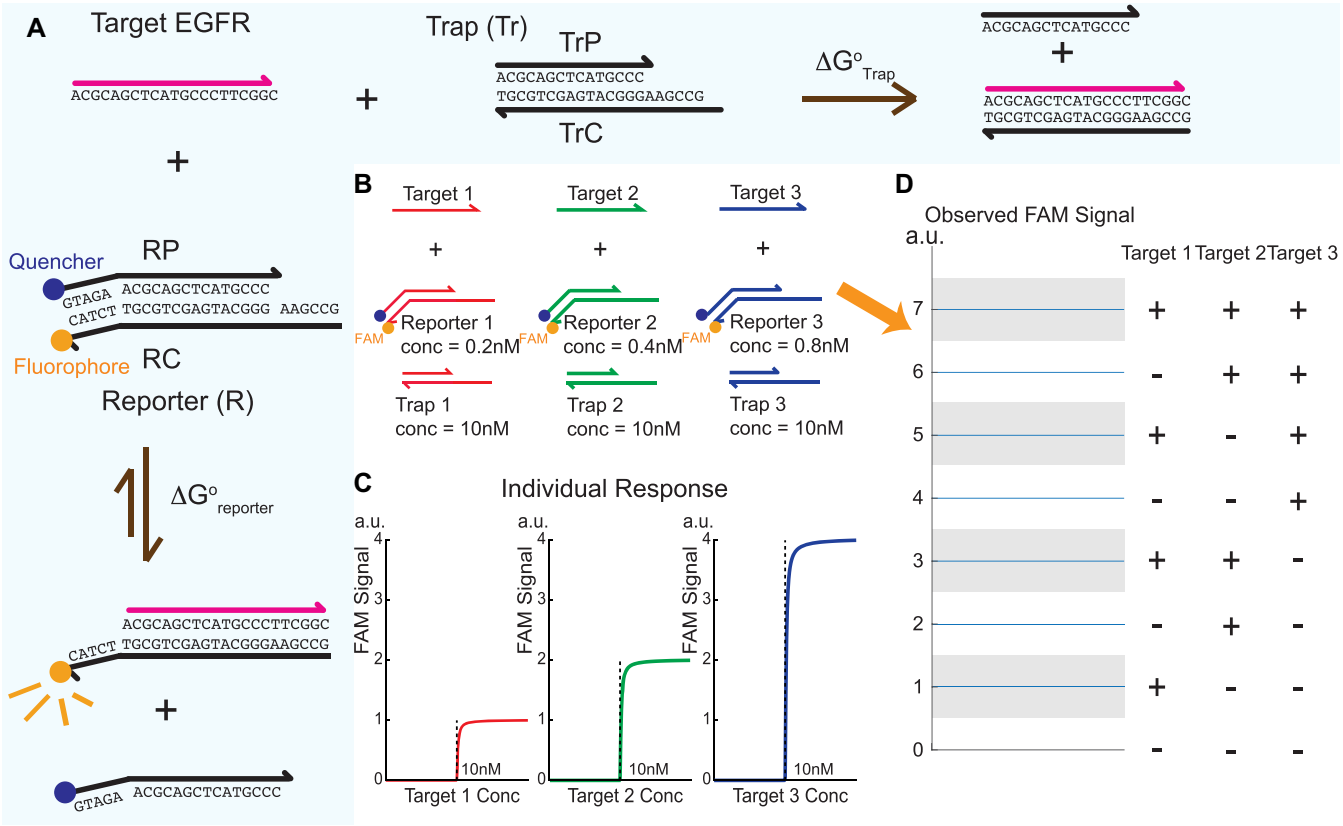

Figure 2. Analog-to-multiple-digital conversion using toehold probe-based DNA detection systems. (**A**) Schematics of one Trap and Reporter system. Both Trap and Reporter are toehold probes perfectly matched to the 21 nt target sequence from the EGFR gene sequence. Trap binds to the target with a more negative reaction free energy ($\Delta G^{\circ}_{\text{Trap}}$) than the Reporter ($\Delta G^{\circ}_{\text{Reporter}}$), thus the target will preferably bind to the Trap until all Trap probes are exhausted. The RC and RP strands in the Reporter are respectively modified with a fluorophore and a quencher. The detection threshold is set based on Trap concentration: the observation of a baseline signal represents low input (target concentration $[T]_0$ lower than Trap concentration $[Tr]_0$), when Reporter is quenched; the observation of a maximal signal represents high input ($[T]_0 > [Tr]_0$), when the Reporter is activated. Because the Reporter concentration is much lower than the detection threshold, the grayzone is narrow. (**B**) Example schematic of a 3-dimension system for simultaneous analysis of three different DNA targets. To analyze the status of three DNA Targets, three Traps and three Reporters are introduced. Each Reporter and Trap specifically hybridizes to its respective Target; the same fluorophore is used on all Reporters (FAM in this example). Reporter concentrations are assigned with a power-of-2 scheme: Reporter 1 (for Target 1) has a concentration of 0.2 nM; Reporter 2 (for Target 2) has $2^1 \times 0.2$ nM $= 0.4$ nM; Reporter 3 (for Target 3) has $2^2 \times 0.2$ nM $= 0.8$ nM. Trap concentrations are the detection threshold concentrations for their respective targets; Trap concentrations are much higher than their corresponding Reporter concentrations. (**C**) Individual response curve of each Trap and Reporter pair. All three dimensions emit digital FAM signals when their target concentrations exceed respective thresholds. FAM signals emitted are 1, 2 and 4 a.u. (**D**) Infer the status of three targets from eight levels of FAM signals. Each possible observed signal can only correspond to one status combination of the three targets. For example, if we observe 7 a.u. of FAM signal, we infer the Targets that are above threshold are Target 1,Target 2 and Target 3 [7 = 1 + 2 + 4]. If we observe 3 a.u. of FAM signal, we infer the Targets that are above threshold are Target 1 and Target 2 [3 = 1 + 2].

In this article, we first designed the Reporter–Trap pairs based on simulation results of reaction thermodynamics and kinetics, and then experimentally characterized each of the response functions. We next combined different Reporter–Trap pairs and experimentally achieved compressed encoding of $D = 4$ dimensions (targets) in one fluorescence channel. Because the noise was greater and the grayzones were wider in experiments than in theory, due to variation in pipetting and imperfect DNA synthesis etc., the achievable D number was lower than the theoretical value. We also performed a blinded experiment to determine the concentration status (above or below threshold) of seven different targets in five samples; the concentrations were unknown to the experimenter. All concentration status was correctly identified. The fluorescent probe-based DNA detection is just a model system to demonstrate our theory of compressed encoding. The same principle can be applied to other types of sensors, such as electronic, magnetic and pH sensors, as well as other types of detection, such as protein and metabolite detection.

MATERIALS AND METHODS

Oligo synthesis and storage conditions

Oligonucleotide molecules used in this study were purchased from Integrated DNA Technologies (IDT). All non-modified oligos were ordered with standard desalting. All oligos with fluorophore or quencher modifications were ordered with post-synthesis HPLC purification. All oligos were sequence-verified by IDT via mass spectrometry; purified oligos were also subject to size verification by capillary electrophoresis. The sequence of each oligo can be

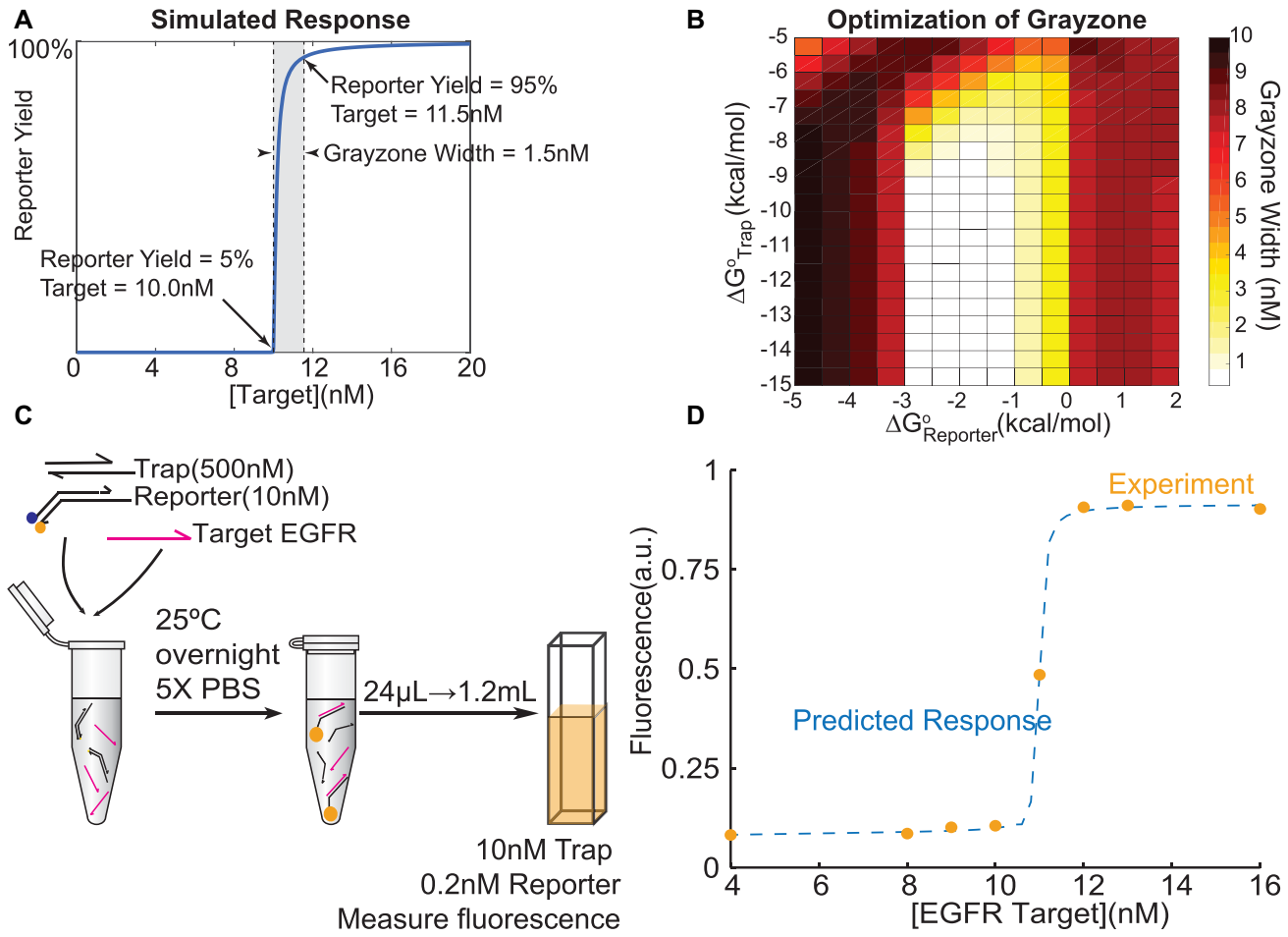

Figure 3. Characterization of step function response by toehold probe-based DNA detection system. (**A**) Simulation result of 10 nM Reporter ($\Delta G^{\circ}_{\text{Reporter}} = -1$ kcal/mol) and 500 nM Trap ($\Delta G^{\circ}_{\text{Trap}} = -11.3$ kcal/mol) reacting at 25°C for 16 h. Target concentration ranging from 5 to 95% maximal signal is defined as the grayzone (grayzone = 1.5 nM). (**B**) Simulation results of different combinations of $\Delta G^{\circ}_{\text{Reporter}}$ and $\Delta G^{\circ}_{\text{Trap}}$ show an optimal region (dark blue) with the minimized grayzone. Concentrations, temperature and time are the same as in (A). (**C**) Schematic of experimental procedures. Target, Trap and Reporter were mixed in 5× PBS and incubated at 25°C for 16 h; then the solution was diluted 50×, and the fluorescence was measured. (**D**) Experimental fluorescence (orange dots) generated by different amount of target inputs using the conditions in (C). Dashed blue line shows the predicted (fitted) response curve based on the best-fit Trap concentration of 10.7 nM. Minimal rather than no fluorescence was still noticed that increased as the target concentration increased before Trap is consumed.

found in Supplementary Materials S5 (Supplementary Table S5-1). All oligos were originally pre-suspended by IDT in Tris·EDTA (pH = 8.0) buffer at roughly 100 μM; stock solutions were stored at 4°C until use.

Toehold probe formulation

All the strands were re-quantified using Nanodrop. A total of 1 μM Reporter probe stock solutions and 5 μM Trap probe stock solutions were formulated by mixing each protector strand (toehold probe upper strand) with each complement strand (toehold probe lower strand) at a 2:1 ratio; 1 μM toehold probe means 1 μM complement and 2 μM protector. Then, we performed thermal annealing for the probe solution using Eppendorf MasterCycler Personal Thermocyclers, following a program of initial denaturing at 95°C for 5 min and subsequent uniform cooling down to 20°C over 75 min. Annealed probes were stored at 4°C until use.

Protocol for reaction and fluorescence measurement

Probes were mixed with targets in 5×PBS (phosphate-buffered saline) buffer. Concentrations in reaction tubes were 50× of the measured final concentrations. For example, in Figure 4C, all final Trap concentrations were 10 nM, and final Reporter concentrations of CYCS, VEGFA, KRAS and CFTR were 0.2, 0.4, 0.8 and 1.6 nM, respectively. Thus when performing reactions, all Trap concentrations were 500 nM, with CYCS, VEGFA, KRAS and CFTR Reporter concentrations at 10, 20, 40 and 80 nM. Then the reaction mixture was incubated at room temperature (25°C) in a dark box overnight (roughly 16 h). Next day, 24 μl of reaction was pipetted into 1.2 ml 5×PBS in cuvette for fluorescence measurement. Fluorescence measurements (Figures 3D, 4B and C, and 5A and B) were performed using a Horiba Fluoromax 4 spectrofluorometer and Hellma Semi-Micro 114F spectrofluorometer cuvettes. For data ac-

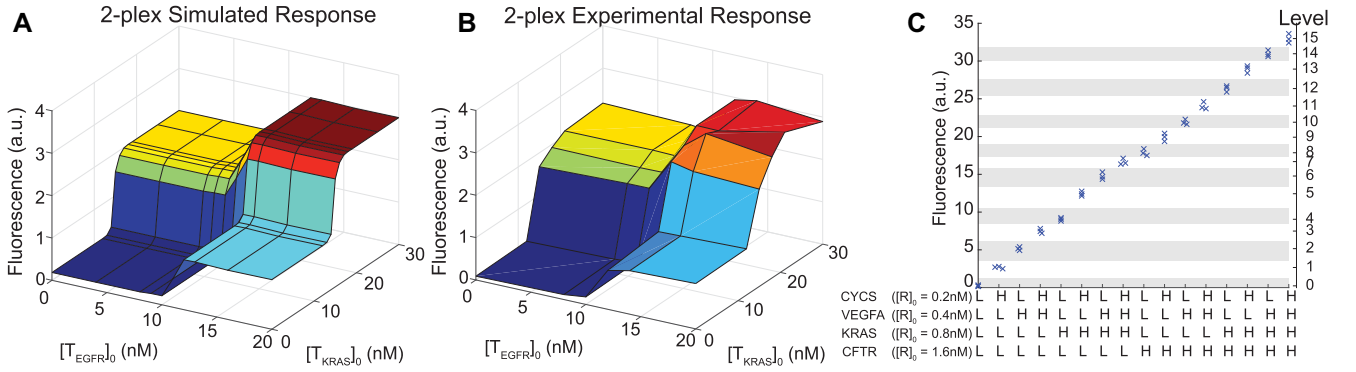

Figure 4. Multiplexed detection of different DNA targets in a single fluorescence channel. (**A**) Simulated response of multiplexed detection of T_{EGFR} and T_{KRAS}. Ordinary Differential Equation (ODE) kinetics simulation was performed with combinations of different input target concentrations to predict fluorescence signal after 16 h of reaction. Reaction conditions and concentrations were the same as (**B**). (**B**) Experimental response of multiplexed detection of two DNA targets (T_{EGFR} and T_{KRAS}, from gene EGFR and KRAS, respectively). Both Reporters were modified with the ROX fluorophore. Concentrations of Traps and Reporters were: $[Tr_{EGFR}]_0 = 10$ nM, $[R_{EGFR}]_0 = 0.2$ nM, $[Tr_{KRAS}]_0 = 15$ nM, $[R_{KRAS}]_0 = 0.4$ nM; different combinations of the two target concentrations were tested. Reaction was performed at 50× of the above concentrations and incubated at 25°C for 16 h in 5× PBS; it was then diluted 50× and the fluorescence was measured. Four distinguishable stages were observed. Fluorescence generated by 0.2 nM Reporter was defined as one fluorescence unit, so with only $[T_{EGFR}]$ above threshold, we observed 1 unit signal; with $[T_{KRAS}]$ above threshold, we observed two units; with both targets above threshold, we observed three units; with both targets below threshold, we observed baseline signal which was below 0.05 unit. Experimental results were consistent with the ODE simulations. (**C**) Experimental demonstration of 4-plex multiplexing in a single FAM fluorescence channel. All Trap concentrations were 10 nM. Reporter concentrations of targets CYCS, VEGFA, KRAS and CFTR were 0.2, 0.4, 0.8 and 1.6 nM, respectively. Final target concentrations were 2 nM for L(Low) and 20 nM for H(High). Results of triplicate experiments are shown as cross symbols. Signals between 16 levels were clearly distinguished. Boundaries of each level are indicated by gray/white zones (see statistical analysis and boundary calculation in Supplementary Materials S3, Table S3-1 and Figure S3-1). Background signal was the fluorescence of the reaction mix containing all Reporters and Traps in the absence of target; All fluorescence signals collected were background-subtracted.

quisition, excitation and emission wavelengths were set at 582 and 600 nm to generate optimal fluorescence signal for ROX fluorophore; at 495 and 520 nm for FAM fluorophore; at 648 and 668 nm for Cy5 fluorophore. Slit sizes were set at 4 nm for both excitation and emission, and integration time was 10 s (per cuvette) with a 60 s integration interval between each two periods. Ten continuous data points were collected (60 s per data point) in each cuvette. Reaction temperature during fluorescence measurement was controlled at 25°C by an external water bath purchased from Thermo Fisher Scientific. The fluorescence signal of each sample was calculated as the mean of the last five reads. All fluorescence signals collected were corrected for position (Supplementary Materials S3).

RESULTS

Implementation of step function response

Here we achieve a step function response using a toehold probe-based DNA detection system. The Trap and Reporter is a pair of competitive composition binding to the same target sequence. A competitive composition schematic with Trap and Reporter is shown in Figure 2A; the Trap implementation is similar to previously reported thresholding methods by Qian *et al.* (15) and Seelig *et al.* (16). Both Trap and Reporter are toehold probes that can perfectly bind to target sequence (T) following the chemical equations:

$$T + P_{Tr} \cdot C_{Tr} \rightleftharpoons T \cdot C_{Tr} + P_{Tr} \qquad \Delta G^{\circ}_{Trap} \qquad (3)$$

$$T + P_{R} \cdot C_{R} \rightleftharpoons T \cdot C_{R} + P_{R} \qquad \Delta G^{\circ}_{Reporter} \qquad (4)$$

Each target molecule can exist in one of the three states: unbound (T), bound to the Trap ($T \cdot C_{Tr}$) or bound to the Reporter ($T \cdot C_{R}$). The occupancy of each state follow a Boltzmann distribution based on the ΔG°_{Trap} and $\Delta G^{\circ}_{Reporter}$. The standard free energy of reaction (3) (ΔG°_{Trap}) is more negative (favorable) than that of reaction (4) ($\Delta G^{\circ}_{Reporter}$), in order for the target molecules to preferentially stay in the state of bound to the Trap ($T \cdot C_{Tr}$) until all Trap molecules are exhausted.

In Figure 2A, both Trap and Reporter are toehold probes (13) perfectly matched to the 21-nt target sequence from the EGFR (17) gene sequence. Our design for the sequences of the probes and protectors was based on the thermodynamic parameters in reference (18) and design principles in reference (13). The binding energies between fluorophores and quenchers are: $\Delta G^{\circ}_{ROX\text{-}RQ} = -3.5$ kcal/mol, $\Delta G^{\circ}_{FAM\text{-}FQ} = -3.25$ kcal/mol, $\Delta G^{\circ}_{Cy5\text{-}RQ} = -3.8$ kcal/mol based on our unpublished experimental data obtained according to reference (19).

Each toehold probe consists of an upper and a lower oligo. The upper oligo is shorter than the lower oligo by a number of nucleotides; the single-stranded nucleotides on the right-most lower strand are referred to as the *toehold* (20). The lower oligo has sequence complementary to subsequences of the target, which is called complement; and the upper oligo has sequence identical to subsequences of the target, which is called protector. The RC and RP strands in the Reporter are respectively modified with a fluorophore and a quencher. In the kinetics process, the target will first react proportionally with both the Trap and the Reporter. However, the Reporter reaction is reversible and Reporter will re-release the target, while the Trap permanently binds to the target. At equilibrium, we will not notice any fluorescence until the Trap is used up and the Reporter starts

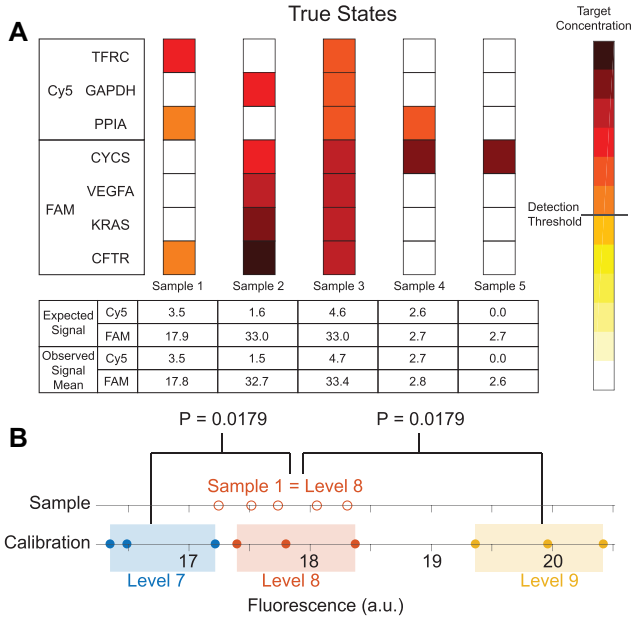

Figure 5. 7-plex blinded sample testing. (**A**) Seven-plex Trap and Reporter systems were used, each targeting an ≈25 nt sequence in a different gene. TFRC, GAPDH and PPIA targets were reported by the Cy5 channel; CYCS, VEGFA, KRAS and CFTR targets were reported by the FAM channel. Detection threshold for each target was 10 nM. The characterization results of FAM system are shown in Figure 4C. The characterization results of Cy5 system are shown in Supplementary Materials S4 (Supplementary Figure S4-1). The target concentration had two levels: above threshold or below threshold; five samples were prepared to have five different level combinations out of the $2^7 = 128$ possible combinations. Above-threshold target concentrations ranged from 10 to 22 nM. The samples were prepared by ZZ, and the tests were performed by author YHY; target concentrations were unknown to YHY until the fluorescence results were obtained. All five blinded samples were tested in quintuplicate. The observed signal levels were consistent with the expected signal levels. (**B**) An example of analysis of sample 1 in FAM channel using distribution free statistics. The quintuplicate datapoints of sample fluorescence are shown as hollow red dots, and the calibration datapoints (triplicates) are shown as solid dots. All five sample datapoints were significantly above all three Level 7 calibration datapoints (P-value = 0.0179 calculated using distribution free statistics); All five sample datapoints were significantly below all three Level 9 calibration datapoints (P-value = 0.0179 calculated using distribution free statistics); so the sample content was most likely to be the same as Level 8 (i.e. high CFTR, low CYCS, low VEGFA, low KRAS).

to occupy the target (Supplementary Materials S2 and Figures S2-1). Both the Reporter and the Trap may adopt a large number of architectures, including molecular beacon (21) or M-Probe (22) as reported in previous literature.

To simultaneously analyze k different DNA targets, we introduce k Traps and k Reporters. Each Reporter and Trap specifically hybridizes to its respective target. Reporter concentrations are assigned with a power-of-2 scheme to reach a power-of-2 fluorescence intensity for each above-threshold target. The same fluorophore is used on all Reporters. Figure 2B and C shows an example of a three-dimension system design for simultaneous analysis of three different DNA targets. In this example, 0.2 nM of Reporter 1 generates 1 arbitrary unit (a.u.) of fluorescence signal. Then 0.4 nM Reporter 2 generates 2 a.u. fluorescence signal, while 0.8 nM Reporter 3 generates 4 a.u. fluorescence signal. In this case, the possible observed fluorescence levels are $2^3 = 8$ different values evenly spaced between 0 a.u. and 7 a.u. Each fluorescence value can only represent one combination of three targets (Figure 2D).

Threshold values can be individually programmed for each target by setting individual Trap concentration. We can set any desired thresholds for different input analytes; we will show experiments with varying thresholds on different inputs later (in Figure 4B the thresholds are different for the two targets; in Figure 4C the thresholds are equal for the four targets). To achieve the desired digital response, Trap concentration should be much higher than the corresponding Reporter concentration so that Reporter concentration is negligible compared to detection threshold (see Supplementary Materials S1 and Figure S1-2 for the recommended rules of setting thresholds and Reporter concentrations).

To provide a quantitative guidance for competitive composition designs, we constructed an ordinary differential equation model of the two reactions involved. The rate constants of all forward reactions are assumed to be $k_+ = 3\times10^6 M^{-1}s^{-1}$ based on previous literature (20,23), and the rate constants of the reverse reactions are calculated based on the equilibrium constants and the assumed forward rate constant, as follows:

$$k_{\text{Trap-}} = \frac{k_+}{K_{\text{eq(Trap)}}} = k_+ e^{\frac{\Delta G^\circ_{\text{Trap}}}{R\tau}} \quad (5)$$

$$k_{\text{Reporter-}} = \frac{k_+}{K_{\text{eq(Reporter)}}} = k_+ e^{\frac{\Delta G^\circ_{\text{Reporter}}}{R\tau}} \quad (6)$$

where R is the ideal gas constant and τ is the temperature in Kelvin. All corresponding ordinary differential equations and simulation details are in Supplementary Materials S1.

Figure 3A shows the kinetics simulation with 10 nM Reporter ($\Delta G^\circ_{\text{Reporter}} = -1$ kcal/mol) and 500 nM Trap ($\Delta G^\circ_{\text{Trap}} = -11.3$ kcal/mol) reacting at 25°C for 16 h followed by 50× dilution, resulting in 0.2 nM Reporter and 10 nM Trap. A digital step function response was mimicked. When target concentration $[T]_0$ was lower than Trap concentration $[Tr]_0 = 10$ nM, Reporter was quenched and baseline signal was observed; with high input $[T]_0 > [Tr]_0 = 10$ nM, Reporter was activated and maximal signal was observed. Target concentration ranging from 5 to 95% maximal signal was defined as the grayzone. $[T]_0 = 10.0$ nM when Reporter yield = 5%; $[T]_0 = 11.5$ nM when Reporter yield = 95%. The grayzone width = 11.5 − 10.0 nM = 1.5 nM.

Our kinetic simulations thus suggest the optimal $\Delta G^\circ_{\text{rxn}}$ of the Reporter and Trap (Figure 3B) with minimized grayzone, which in turn guides a sequence-level design. Under this reaction condition, when $\Delta G^\circ_{\text{Reporter}}$ is in the range of −3 to −1 kcal/mol and $\Delta G^\circ_{\text{Trap}}$ is more negative than −9 kcal/mol, the grayzone will be <1 nM. The optimal region of $\Delta G^\circ_{\text{rxn}}$ is very wide, indicating that the system can tolerate inaccuracies in probe sequence design. Individual simulated response curves with different combinations of $\Delta G^\circ_{\text{Reporter}}$ and $\Delta G^\circ_{\text{Trap}}$ are shown in Supplementary Materials S1 (Supplementary Figure S1-1).

Next, we experimentally characterized the response of the Trap and Reporter system. Figure 3C and D shows the characterization of Trap and Reporter system that targeted a

synthetic oligonucleotide from EGFR subsequence shown in Figure 2A. Target, Trap and Reporter were mixed in 5× PBS and incubated at 25°C for 16 h. Then the solution was diluted 50×, and the fluorescence was measured. The toehold probe displacement reaction has a speed comparable to that of direct hybridization, given a single-stranded toehold of sufficient length (20). Based on our experimental measurement of system kinetics (Supplementary Materials S2 and Figure S2-1), we believe the system will reach equilibrium at this condition.

With constant Trap (10 nM) and Reporter (0.2 nM) concentrations, final target concentrations range from 4 to 16 nM. Target detection threshold is 10 nM, which is set by final Trap concentration. Figure 3D is the example of experimental fluorescence (orange dots) generated by different amount of target inputs using the sequences in Figure 2A and under the condition in Figure 3C. We observed a big fluorescence jump from baseline fluorescence at 10 nM to near maximal fluorescence at 12 nM, with a grayzone of less than 2 nM. The dashed blue line shows the predicted response curve fitted with the eight experimental values (orange dots) based on the best-fit Trap concentration of 10.7 nM. The experimental results perfectly mimiced the simulated step function response.

Demonstration of single-channel multiplexing

After demonstrating analog-to-digital conversion with one DNA target and obtaining step function response, we continued with multiplex signal analysis in a single channel. We started with a 2-Plex system which allowed for easy visualization of the analog-to-two-digital conversion response curve. With 2-Plex (Input 1 and Input 2), we expected to observe four stages of output signal levels, corresponding to four status: Low Input 1, Low Input 2; High Input 1, Low Input 2; Low Input 1, High Input 2; High Input 1, High Input 2.

To show sequence generality of the Trap and Reporter approach, we constructed a new system targeting a subsequence of KRAS (24) gene. KRAS Trap concentration $[Tr_{KRAS}]_0$ was 15 nM, KRAS Reporter concentration $[R_{KRAS}]_0$ was 0.4 nM. With KRAS target concentrations ranging from 0 to 30 nM, a step function response was observed for the KRAS target with a threshold of 15 nM, indicating that we could easily adjust thresholds by changing the Trap concentrations.

Here, we used $I_H - I_L = 2^{(k-1)} I_{au}$ for the step function of the kth input, so that the signal levels were evenly spaced. For Input 1 we used $[R_{EGFR}]_0 = 0.2$ nM; For Input 2 we used $[R_{KRAS}]_0 = 0.4$ nM. In this case, I_{au} was the signal generated by 0.2 nM of ROX fluorophore. Four distinguishable fluorescence stages were predicted by Ordinary Differential Equation (ODE) kinetics simulation (Figure 4A). Simulation was based on the ΔG°_{Trap} and $\Delta G^\circ_{Reporter}$ calculated from DNA sequences used in actual experiments.

Experimental response of multiplexed detection of two DNA targets (T_{EGFR} and T_{KRAS}) is shown in Figure 4B. Different concentration combinations of the two target were tested by reacting each target combination with the constant 2-set Trap and Reporter system in the same tube. EGFR target concentration ranged from 0 to 20 nM, with a detection threshold of 10 nM set by EGFR Trap concentration; KRAS target concentration ranged from 0 to 30 nM, with a detection threshold of 15 nM set by KRAS Trap concentration. Both Reporters were modified with the ROX fluorophore. Fluorescence generated by 0.2 nM reporter was defined as one fluorescence unit. With only $[T_{EGFR}]$ above threshold, we observed one unit signal; with $[T_{KRAS}]$ above threshold, we observed two units; with both targets above threshold, we observed three units; with both targets below threshold, we observed baseline signal which was below 0.05 unit. Four distinguishable fluorescence stages perfectly matched with the simulation. There were grayzones of less than 2 nM in EGFR dimension and <3 nM in KRAS dimension. The upper right corner of Figure 4B experimental data resembled Figure 4A simulation less than the rest parts, since superposition of multiple response curves introduced errors especially when signals were at high level (in this case both targets were above thresholds).

Typical qPCR machines have four to five fluorescence channels for detecting four to five different DNA targets. We next performed homogeneous multiplexing analysis comparable to a qPCR machine using a single fluorescence channel with our system. We chose four different targets. Each target was an ≈25 nt subsequence of a different gene (CYCS, VEGFA, KRAS and CFTR). We designed a Trap and Reporter system for each of them. Figure 4C shows experimental results demonstrating a 4-plex multiplexing system in a single FAM fluorescence channel. All Trap concentrations were 10 nM. Reporter concentrations of targets CYCS, VEGFA, KRAS and CFTR were 0.2, 0.4, 0.8 and 1.6 nM, respectively. This 4-plex Trap and Reporter system was designed to showcase a digital signal space with $N = 16$ levels, which could represent the binary information of four different inputs; each of the $2^4 = 16$ possible combinations had a corresponding digital signal level. With four-dimensional inputs, we were unable to show response curves like with one-dimensional (Figure 3D) or two-dimensional (Figure 4B) inputs, so we did not test a range of target concentrations spanning from below threshold to above threshold; instead, for all 16 possible combinations we assigned a final target concentration: 2 nM for Low (below threshold) and 20 nM for High (above threshold). Each combination could have Low or High for each target, which was representative of its respective signal level.

As shown in Figure 4C, signals of 16 levels were clearly distinguished, as we expected in Figure 1B. The system could perform homogeneous multiplexing analysis comparable to qPCR capability. Note that all results shown here came from our first design. We did not conduct any sequence adjustment, stoichiometric tuning or empirical Trap/Reporter concentration adjustment. Our system is robust because there's a wide optimal ΔG°_{rxn} region that can realize step function responses with small grayzones.

We also performed 3-plex multiplexing using a single FAM fluorescence channel with Qubit 3.0 fluorometer, which had worse detection limit and lower dynamic range than the spectrofluorometer. Signals of 8 different levels were clearly distinguished (see Supplementary Materials S3 and Figure S3-2).

Multiplexed DNA detection with multiple fluorescence channels

To prove that we could determine the status of multiple targets by one-dimensional fluorescence intensity, we performed blinded experiment. We constructed a 7-plex Trap and Reporter system, containing seven Trap-Reporter sets, with each set targeting an ≈25 nt subsequence in a different gene. The 7-plex system was the combination of a 1-analog-to-4-digitals system and a 1-analog-to-3-digitals system. CYCS, VEGFA, KRAS and CFTR targets were reported by the FAM channel (with Figure 4C as calibration); TFRC, GAPDH and PPIA targets were reported by the Cy5 channel (calibration in Supplementary Materials S4 and Figure S4-1). Detection threshold was the same for each target, which was 10 nM; Each target could have a concentration of above threshold or below threshold. This system enabled simultaneous determination of concentration status (above threshold or below threshold) of seven different targets in a homogeneous reaction.

To perform the blinded experiment for determining the concentration status (above or below threshold), ZZ (the preparer) prepared five samples, each with varied concentrations of seven different targets (Supplementary Table S4-1). The concentrations were unknown to YHY (the experimenter). Each target had two concentration levels: above threshold or below threshold; Five blinded samples were prepared to have five different level combinations out of the $2^7 = 128$ possible combinations. Above-threshold target concentrations were prepared to be ranging from 10 to 22 nM. Below-threshold target concentrations were prepared to be 0 nM. Each sample reacted with 7-plex Trap and Reporter system in the same tube at 25°C for 16 h, and then the target combination of each sample was determined by measuring the fluorescence endpoint at FAM and Cy5 channel in fluorometer. All five blinded samples were tested in quintuplicate. The FAM and Cy5 fluorescence endpoints were used to infer the initial status of each sample. We extrapolated the combination of CYCS, VEGFA, KRAS and CFTR in the sample based only on FAM channel fluorescence intensity, and the combination of TFRC, GAPDH and PPIA in the sample based only on Cy5 channel fluorescence. As shown in Figure 5A, all five status was successfully and correctly determined by YHY (the experimenter). The expected signal and the observed signal for each sample were consistent.

Since each signal level within the same channel corresponded to a unique target combination, if we could determine the signal level, we could infer the concentration status of targets of a blinded sample. Each calibration was triplicated (three datapoints); each sample test was quintuplicate (five datapoints). Figure 5B shows an example of analysis of sample 1 in FAM channel using distribution free statistics. The range of each level was from the lowest to the highest calibration datapoints. Here, four out of five sample datapoints were distributed in the range of Level 8, so the sample content was most likely to be the same as Level 8 (i.e. high CFTR, low CYCS, low VEGFA, low KRAS). In addition, five sample datapoints were significantly different from Level 7 calibration range and Level 9 calibration range. The *P*-value of sample 1 in Level 7 was calculated as the probability of all five sample datapoints falling above all three Level 7 calibration datapoints: $P = (3! \times 5!)/(8!) = 0.0179$; the *P*-value of sample 1 in Level 9 was calculated using the same method. Because we did not think the measured fluorescence would follow a normal distribution, we used distribution free statistics in this analysis.

Note that FAM channel results of sample 1 we have shown here is the most ambiguous case as the step size from Level 7 calibration to Level 8 calibration was not big enough. All other samples' FAM channel results and all five samples' Cy5 channel results fell in respective levels with big distances from other levels, enabling clearer concentration determinations. The complete analysis results can be found in Supplementary Materials S4 (Supplementary Figure S4-2).

Likewise, sample 1's Cy5 channel was determined to be Level 5 (i.e. high TFRC, low GAPDH, high PPIA), thus the status of sample 1 was inferred to be high TFRC, low GAPDH, high PPIA, low CYCS, low VEGFA, low KRAS, high CFTR. As a result, YHY correctly determined all target concentration status unknown to her based on fluorescence intensity from two channels.

DISCUSSION

We have introduced the theoretical framework of the analog-to-multiple-digital signal conversion, and demonstrated a chemical implementation for assessing whether multiple DNA sequence analytes exceeded their respective programmed threshold values. Using a single fluorescence channel, we were able to analyze concentration status of 4 DNA targets. With two channels we demonstrated the correct interpretation of concentration status of seven DNA targets under blinded conditions. Although there are a variety of analog computing devices utilizing DNA strand displacement reactions (25,26), we are not aware of any previous work that makes use of the analog-to-multiple-digital signal conversion concept in chemistry or biological engineering. Though we currently demonstrated the concept with DNA and the fluorescence, we believe that the same concept can be generalized and applied to other analytes such as proteins and metabolites.

To translate the concept into a viable biochemical or biomedical diagnostics, the DNA limit of detection should be significantly lower than the nanomolar ranges listed in this paper that serve as proof-of-concept demonstrations. Here, we used a fluorometer as our readout, which allowed for multiple analog fluorescence channels, but had a poor limit of detection. Sensors exhibiting femtomolar to attomolar levels of DNA sensitivity (e.g. based on electrochemistry, whispering gallery mode resonators, nanoparticle-induced fluorescence enhancement or single molecule imaging) could realize the direct multiplexed reporting of DNA analytes at biologically relevant concentrations without amplification.

Alternatively, the DNA analytes could be pre-amplified and the amplicons can be subject to the analog-to-multiple-digital conversion. For this usage, PCR is not recommended because of well documented sequence bias in PCR amplification efficiency (27–29), which grows exponentially with

the number of PCR cycles. More uniform DNA amplification techniques (e.g. rolling circle amplification (30) and multiple displacement amplification (31,32)) may be suitable.

One strength of our theoretical framework is that the sensor used only requires a large dynamic range, but not necessarily linear responses. Analog-to-multiple-digital conversion can be achieved as long as the observed analog signal can be discretized into different steps to represent different combinations of digital information, though general more complex chemical implementations. Because far more sensors exhibit non-linear responses than linear responses (e.g. electrochemical sensors (33) and AuNP-based fluorescent nanobeacons (34)), we envision this feature will be an advantage for translating to diagnostic applications.

SUPPLEMENTARY DATA

Supplementary Data are available at NAR online.

ACKNOWLEDGEMENTS

The authors thank Zhuo Zhang from Hong Kong University of Science and Technology for blinded sample preparation. The authors thank Jianyi Nie and Peng Dai for proofreading assistance. The authors thank Juexiao Sherry Wang for discussions.

Authors' contributions: Y.H.Y., D.Y.Z. and L.R.W. conceived the project. Y.H.Y. performed experiments and data analysis. Y.H.Y., D.Y.Z. and L.R.W. wrote the manuscript. D.Y.Z. and L.R.W. are corresponding authors.

FUNDING

Cancer Prevention Research Institute of Texas [RP180147 to D.Y.Z.]; National Human Genome Research Institute [R01HG008752 to D.Y.Z.]. Funding for open access charge: National Human Genome Research Institute [R01HG008752 to D.Y.Z.].

Conflict of interest statement. Y.H.Y. is a full-time employee at Nuprobe Global. L.R.W. consults for Nuprobe Global. D.Y.Z. consults for and holds significant equity in Nuprobe Global and Torus Biosystems, and consults for Avenge Bio.

REFERENCES

1. Popowitch,E.B., O'Neill,S.S. and Miller,M.B. (2013) Comparison of the Biofire FilmArray RP, Genmark eSensor RVP, Luminex xTAG RVPv1, and Luminex xTAG RVP fast multiplex assays for detection of respiratory viruses. *J. Clin. Microbiol.*, **51**, 1528–1533.
2. Nie,S., Roth,R.B., Stiles,J., Mikhlina,A., Lu,X., Tang,Y.W. and Babady,N.E. (2014) Evaluation of Alere i Influenza A&B for rapid detection of influenza viruses A and B. *J. Clin. Microbiol.*, **52**, 3339–3344.
3. Beckman,A.O. and Fracker,H.E. (1936) *Apparatus for Testing Acidity*, U.S. Patent 2,058,761.
4. Tarbell,D.S. and Tarbell,A.T. (1980) The development of the pH meter. *J. Chem. Educ.*, **57**, 133–134.
5. Drummond,T.G., Hill,M.G. and Barton,J.K. (2003) Electrochemical DNA sensors. *Nat. Biotechnol.*, **21**, 1192–1199.
6. Das,J., Cederquist,K.B., Zaragoza,A.A., Lee,P.E., Sargent,E.H. and Kelley,S.O. (2012) An ultrasensitive universal detector based on neutralizer displacement. *Nat. Chem.*, **4**, 642–648.
7. Labib,M., Sargent,E.H. and Kelley,S.O. (2016) Electrochemical methods for the analysis of clinically relevant biomolecules. *Chem. Rev.*, **116**, 9001–9090.
8. Engvall,E. and Perlmann,P. (1972) Enzyme-linked immunosorbent assay, ELISA: III. Quantitation of specific antibodies by enzyme-labeled anti-immunoglobulin in antigen-coated tubes. *J. Immunol.*, **109**, 129–135.
9. Lequin,R.M. (2005) Enzyme immunoassay (EIA)/enzyme-linked immunosorbent assay (ELISA). *Clin. Chem.*, **51**, 2415–2418.
10. Sun,Y. and Fan,X. (2011) Optical ring resonators for biochemical and chemical sensing. *Anal. Bioanal. Chem.*, **399**, 205–211.
11. Ramachandran,A., Wang,S., Clarke,J., Ja,S.J., Goad,D., Wald,L. and Gill,D. (2008) A universal biosensing platform based on optical micro-ring resonators. *Biosens. Bioelectron.*, **23**, 939–944.
12. Walden,R.H. (1999) Analog-to-digital converter survey and analysis. *IEEE J. Sel. Areas Commun.*, **17**, 539–550.
13. Zhang,D.Y., Chen,S.X. and Yin,P. (2012) Thermodynamic optimization of nucleic acid hybridization specificity. *Nat. Chem.*, **4**, 208–214.
14. Wu,L.R., Wang,J.S., Fang,J.Z., Evans,E.R., Pinto,A., Pekker,I., Boykin,R., Ngouenet,C., Webster,P.J., Beechem,J. *et al.* (2015) Continuously tunable nucleic acid hybridization probes. *Nat. Methods*, **12**, 1191–1196.
15. Qian,L. and Winfree,E. (2011) Scaling up digital circuit computation with DNA strand displacement cascades. *Science*, **332**, 1196–1201.
16. Seelig,G., Soloveichik,D., Zhang,D.Y. and Winfree,E. (2006) Enzyme-free nucleic acid logic circuits. *Science*, **314**, 1585–1588.
17. Normanno,N., De Luca,A., Bianco,C., Strizzi,L., Mancino,M., Maiello,M.R., Carotenuto,A., De Feo,G., Caponigro,F. and Salomon,D.S. (2006) Epidermal growth factor receptor (EGFR) signaling in cancer. *Gene*, **366**, 2–16.
18. SantaLucia,J. Jr and Hicks,D. (2004) The thermodynamics of DNA structural motifs. *Annu. Rev. Biophys. Biomol. Struct.*, **33**, 415–440.
19. Wang,C., Bae,J.H. and Zhang,D.Y. (2016) Native characterization of nucleic acid motif thermodynamics via non-covalent catalysis. *Nat. Commun.*, **7**, 1–11.
20. Zhang,D.Y. and Winfree,E. (2009) Control of DNA strand displacement kinetics using toehold exchange. *J. Am. Chem. Soc.*, **131**, 17303–17314.
21. Tyagi,S. and Kramer,F.R. (1996) Molecular beacons: probes that fluoresce upon hybridization. *Nat. Biotechnol.*, **14**, 303–308.
22. Wang,J.S., Yan,Y.H. and Zhang,D.Y. (2017) Modular probes for enriching and detecting complex nucleic acid sequences. *Nat. Chem.*, **9**, 1222–1228.
23. Zhang,J.X., Fang,J.Z., Duan,W., Wu,L.R., Zhang,A.W., Dalchau,N., Yordanov,B., Petersen,R., Phillips,A. and Zhang,D.Y. (2018) Predicting DNA hybridization kinetics from sequence. *Nat. Chem.*, **10**, 91–98.
24. Kranenburg,O. (2005) The KRAS oncogene: past, present, and future. *Bio Biophys. Acta*, **1756**, 81–82.
25. Kobayashi,S., Yanagibashi,K., Komiya,K., Fujimoto,K. and Hagiya,M. (2014) Analog DNA computing devices toward the control of molecular robots. *IEEE, 33rd International Symposium on Reliable Distributed Systems Workshops*. pp. 1–11.
26. Song,T., Garg,S., Mokhtar,R., Bui,H. and Reif,J. (2016) Analog computation by DNA strand displacement circuits. *ACS Synth. Biol.*, **5**, 898–912.
27. Kanagawa,T. (2003) Bias and artifacts in multitemplate polymerase chain reactions (PCR). *J. Biosci. Bioeng.*, **96**, 317–323.
28. Acinas,S.G., Sarma-Rupavtarm,R., Klepac-Ceraj,V. and Polz,M.F. (2005) PCR-induced sequence artifacts and bias: insights from comparison of two 16S rRNA clone libraries constructed from the same sample. *Appl. Environ. Microbiol.*, **71**, 8966–8969.
29. Aird,D., Ross,M.G., Chen,W.S., Danielsson,M., Fennell,T., Russ,C., Jaffe,D.B., Nusbaum,C. and Gnirke,A. (2011) Analyzing and minimizing PCR amplification bias in Illumina sequencing libraries. *Genome Biol.*, **12**, R18.
30. Dahl,F., Banr,J., Gullberg,M., Mendel-Hartvig,M., Landegren,U. and Nilsson,M. (2004) Circle-to-circle amplification for precise and sensitive DNA analysis. *Proc. Natl. Acad. Sci. U.S.A.*, **101**, 4548–4553.
31. Dean,F.B., Hosono,S., Fang,L., Wu,X., Faruqi,A.F., Bray-Ward,P., Sun,Z., Zong,Q., Du,Y., Du,J. *et al.* (2002) Comprehensive human

genome amplification using multiple displacement amplification. *Proc. Natl. Acad. Sci. U.S.A.*, **99**, 5261–5266.
32. Pinard,R., de Winter,A., Sarkis,G.J., Gerstein,M.B., Tartaro,K.R., Plant,R.N., Egholm,M., Rothberg,J.M. and Leamon,J.H. (2006) Assessment of whole genome amplification-induced bias through high-throughput, massively parallel whole genome sequencing. *BMC Genomics*, **7**, 216–236.
33. Zuo,X., Song,S., Zhang,J., Pan,D., Wang,L. and Fan,C. (2007) A target-responsive electrochemical aptamer switch (TREAS) for reagentless detection of nanomolar ATP. *J. Am. Chem. Soc.*, **129**, 1042–1043.
34. Li,D., Song,S. and Fan,C. (2010) Target-responsive structural switching for nucleic acid-based sensors. *Acc. Chem. Res.*, **43**, 631–641.